

SUPPLEMENTARY INFORMATION

Transfer RNA-mediated regulation of ribosome dynamics during protein synthesis

Jingyi Fei^{1,3}, Arianne C. Richard^{2,4}, Jonathan E. Bronson^{1,5} & Ruben L. Gonzalez, Jr.¹

¹*Department of Chemistry, Columbia University, New York, NY 10027.*

²*Department of Biological Sciences, Columbia University, New York, NY 10027.*

³*Present address for J.F.: Department of Physics, Center for the Physics of Living Cells, University of Illinois at Urbana-Champaign, Urbana, IL 61801.*

⁴*Present address for A.C.R: Immunoregulation Section, Autoimmunity Branch, National Institute of Arthritis and Musculoskeletal and Skin Diseases, Bethesda, MD 20892.*

⁵*Present address for J.E.B.: Boston Consulting Group, 430 Park Avenue, New York, NY 10022.*

To whom correspondence should be addressed: rlg2118@columbia.edu (R.L.G.).

TABLE OF CONTENTS

Supplementary Figures 1-5

Supplementary Table 1

Supplementary Methods

Supplementary Discussion

SUPPLEMENTARY FIGURES

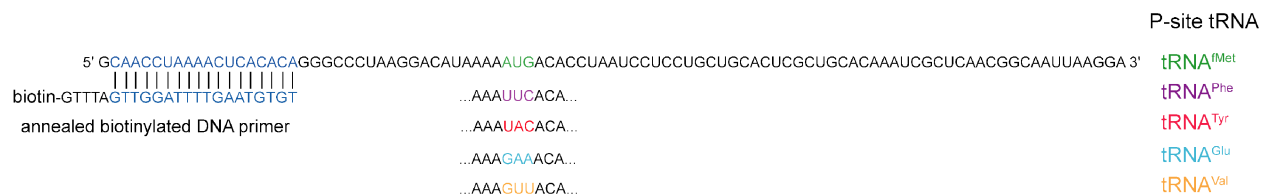


Figure 1. mRNA constructs used to prepare PRE^{-A} complexes.

Five mRNA constructs were designed such that the first codon of the five mRNAs encoded either fMet (green), Phe (purple), Tyr (red), Glu (blue), or Val (yellow), respectively, and no other codons in any of the three reading frames of the mRNAs encoded fMet, Phe, Tyr, Glu, or Val.

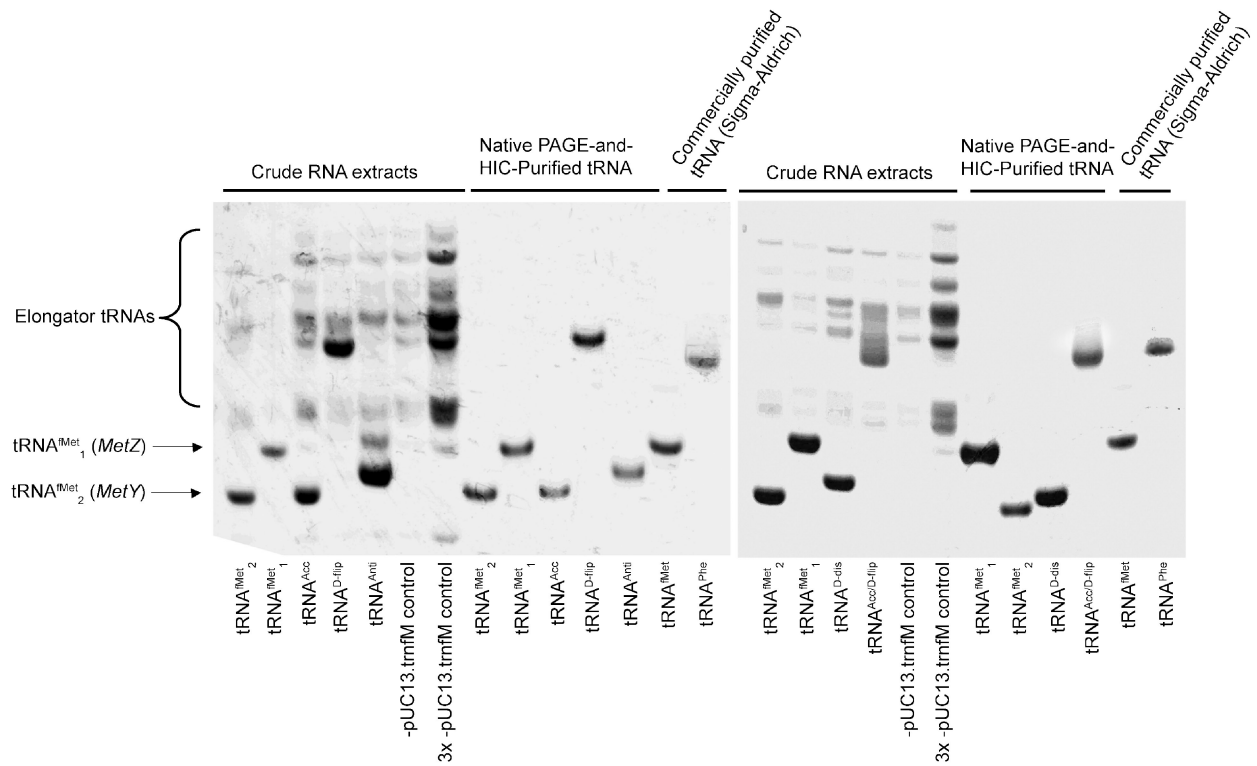


Figure 2. Native polyacrylamide gel electrophoresis (PAGE) analysis of $tRNA^{fMet}$ and $tRNA^{fMet_2}$ mutants. The native PAGE analysis of crude RNA extracts as well as purified tRNAs includes both isoacceptors of initiator $tRNA^{fMet}$ as well as all $tRNA^{fMet_2}$ mutants investigated in this work. The $-pUC13.trnfM$ control refers to a crude RNA extract prepared from *E. coli* strain B105 that had not been transformed with the $pUC13.trnfM$ plasmid. A 3-fold larger amount of the $-pUC13.trnfM$ control was loaded in an additional lane for enhanced visualization of RNA species present at low concentrations. $tRNA^{fMet}$ and $tRNA^{Phe}$ purchased from Sigma-Aldrich serve as markers. The gel was stained with 0.1 % (w/v) toluidine blue.

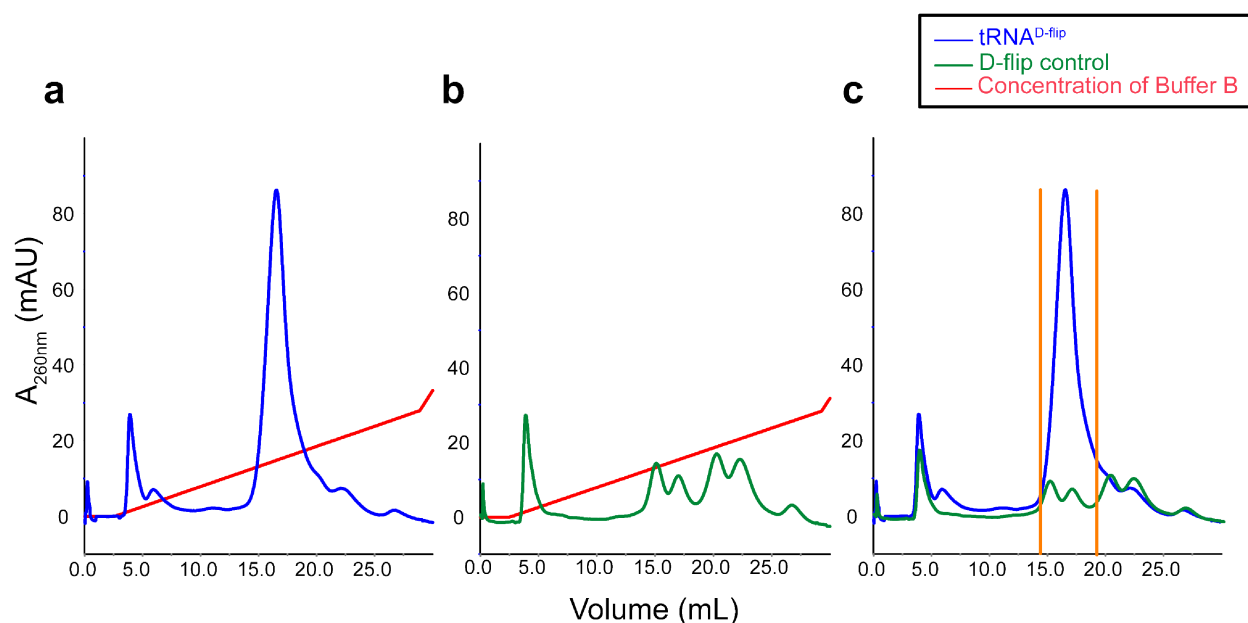


Figure 3. Hydrophobic interaction chromatography (HIC) purification of $tRNA^{D-flip}$. HIC chromatograms were used to estimate the purity of $tRNA^{D-flip}$ and $tRNA^{Acc/D-flip}$, both of which migrate in the same region of the native PAGE as the elongator tRNAs: (a) HIC chromatogram of $tRNA^{D-flip}$; (b) HIC chromatogram of D-flip control tRNA (see Supplementary Methods); (c) overlap of the chromatograms shown in (a) and (b). Based on the peak areas, the contamination of $tRNA^{D-flip}$ with elongator tRNAs is estimated to be <2 %. Fractions between the orange lines were collected, pooled, and used for the aminoacylation and formylation assays described in the Supplementary Methods and Supplementary Figure 4. The purity of $tRNA^{Acc/D-flip}$ was determined in the same way as that described here for $tRNA^{D-flip}$, with the contamination of $tRNA^{Acc/D-flip}$ by elongator tRNAs estimated at <2 % (data not shown).

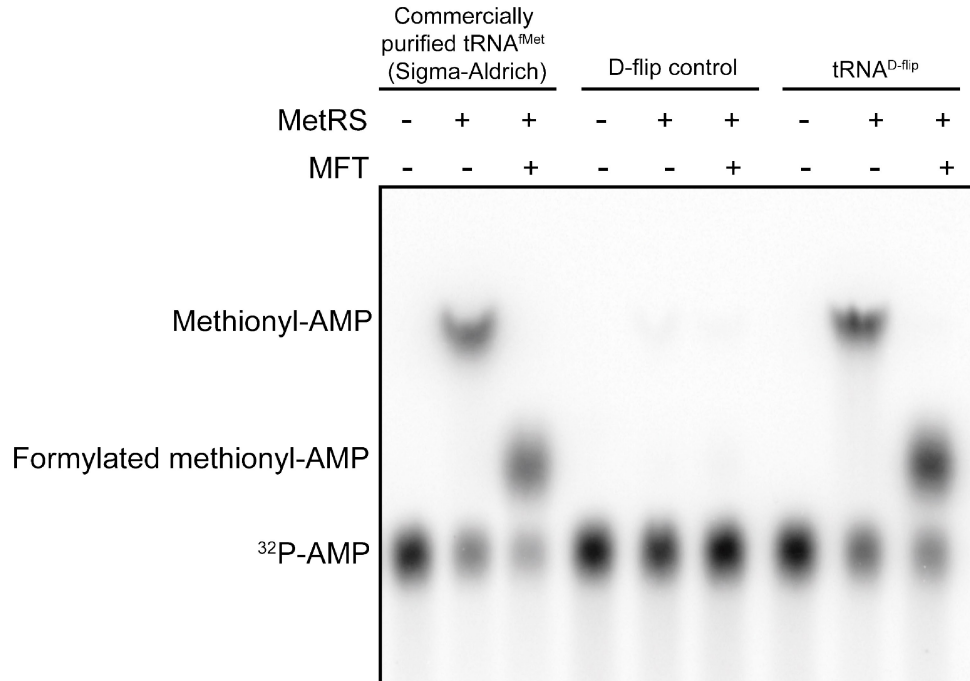


Figure 4. Aminoacylation and formylation analysis of tRNA^{D-flip}.

tRNA^{D-flip} exhibits the same aminoacylation and formylation activity as the wild-type tRNA^{fMet}₁, while D-flip control tRNA (see Supplementary Methods) is not aminoacylated by methionyl-tRNA synthetase or formylated by methionyl-tRNA transformylase to any detectable levels. Based on this result, we conclude that any contaminating elongator tRNAs present in the purified tRNA^{D-flip} sample do not include elongator tRNA^{Met}.

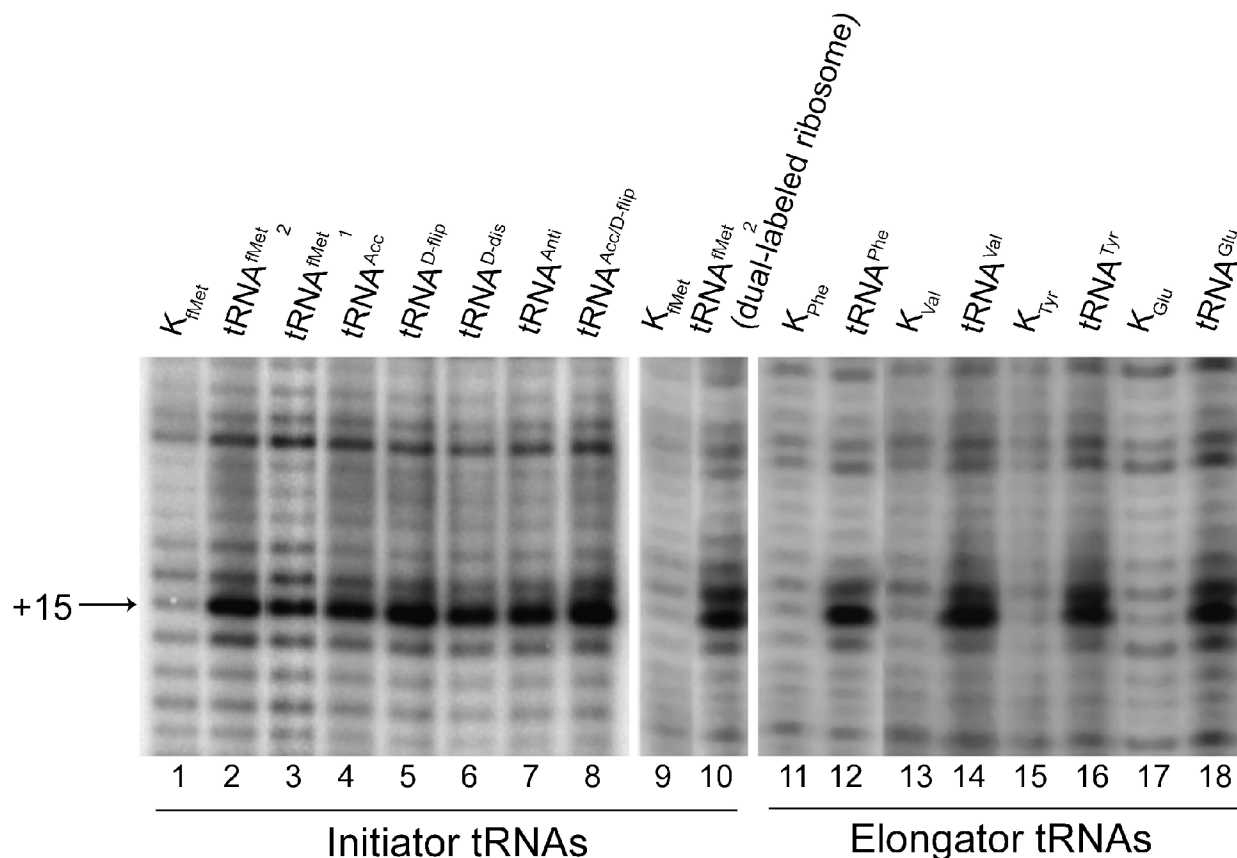


Figure 5. Primer extension inhibition assays for verifying codon-specific binding of tRNAs into the P site of 70S ribosomes.

The ability of wild-type and mutant tRNAs, their corresponding mRNAs, and ribosomal subunits from *E. coli* strain MRE600 to form well-defined PRE^{-A} complexes was tested using a primer extension inhibition assay. The ability of $tRNA^{fMet}_2$, its corresponding mRNA, 30S subunits and dual-labeled 50S subunits from BW25113 to form a PRE^{-A} complex was also tested to ensure that dual-labeled 50S subunits form PRE^{-A} complexes with an efficiency comparable to that observed when using wild-type 50S subunits (Lane 10). Verification that each tRNA and its associated codon were properly positioned within the P site of the corresponding PRE^{-A} complex was achieved through the detection of a strong band at a position on the sequencing gel that is +15 nucleotides downstream of the first nucleotide of the codon located within the P site (i.e. the +15 band). Lanes marked “K” contain control reverse transcription reactions performed for each mRNA construct in the absence of ribosomes and tRNAs. K lanes provide an assessment of the band intensities that result from the stalling or dissociation of reverse transcriptase upon encountering stable mRNA secondary structures intrinsic to each mRNA construct.

SUPPLEMENTARY TABLE

Table 1. Subpopulation analysis of smFRET *versus* time trajectories for PRE^A complexes carrying different P-site tRNAs ^a.

P-site tRNA	SP _{GS1} (%)	SP _{GS2} (%)	SP _{fluct} (%)
PRE^A			
PRE^A_{fMet} complexes			
tRNA ^{fMet} ₁	37±3	4±1	59±4
tRNA ^{fMet} ₂	67±4	3.7±0.9	29±5
PRE^A_{elong} complexes			
tRNA ^{Phe}	8.5±0.1	6±3	85±4
tRNA ^{Tyr}	7±2	8±3	85±2
tRNA ^{Glu}	13±5	3.6±0.7	83±5
tRNA ^{Val}	16±4	6.2±0.9	78±3
PRE^A complexes with tRNA^{fMet} mutants			
tRNA ^{Anti}	68±4	3±1	29±2
tRNA ^{Acc}	58±5	14±3	28±2
tRNA ^{D-flip}	23±3	3.6±0.8	74±3
tRNA ^{D-dis}	35±4	5±2	60±3
tRNA ^{Acc/D-flip}	23±3	13±3	63.5±0.5
PRE^A + 2 μM EF-G(GDPNP)			
PRE^A_{fMet} complexes			
tRNA ^{fMet} ₁	10±1	15±2	75±1
tRNA ^{fMet} ₂	15±3	5.8±0.4	79±3
PRE^A_{elong} complexes			
tRNA ^{Phe}	8±3	78±7	14±5
tRNA ^{Tyr}	9±2	79±6	12±7
tRNA ^{Glu}	9±3	72±6	19±3
tRNA ^{Val}	14±5	66±3	20±4
PRE^A complexes with tRNA^{fMet} mutants			
tRNA ^{Anti}	19±10	6±2	75±9
tRNA ^{Acc}	14±2	32±6	54±4
tRNA ^{D-flip}	8±1	16±7	76±7
tRNA ^{D-dis}	8±1	18±1	74±2
tRNA ^{Acc/D-flip}	4.2±0.4	75±6	20±5

^a The mean and standard deviation (mean ± s.d). of the percentage occupancy of each subpopulation was calculated from three independent data sets. The corresponding bar graphs are shown in Fig. 2b.

SUPPLEMENTARY METHODS

Buffer conditions

Experiments were carried out in Tris-polymix buffer (50 mM Tris acetate (pH_{25°C}=7.0), 100 mM potassium chloride, 5 mM ammonium acetate, 0.5 mM calcium acetate, 0.1 mM ethylenediamine tetraacetic acid, 10 mM 2-mercaptoethanol, 5 mM putrescine dihydrochloride and 1 mM spermidine, free base) at 15 mM magnesium acetate^{1,2}, supplemented with an oxygen-scavenging system (300 µg mL⁻¹ glucose oxidase, 40 µg mL⁻¹ catalase and 1% (w/v) β-D-glucose)²⁻⁴ and a triplet-state quencher cocktail (1 mM 1,3,5,7-cyclooctatetraene (Aldrich) and 1 mM 3-nitrobenzyl alcohol (Fluka))⁵.

Preparation of 30S subunits and L1-L9-labeled 50S subunits

Unlabeled 30S subunits and L1-L9-labeled 50S subunits were prepared as previously described^{4,6}. Briefly, a L1 and L9 double deletion strain was generated from the parent *E. coli* strain BW25113 as previously published^{4,6}. 50S subunits lacking L1 and L9 from this L1 and L9 double deletion strain and 30S subunits from the wild-type strain BW25113 were purified by sucrose density gradient ultracentrifugation using a previously described purification protocol^{2,4,6}. A single-cysteine (Cys) L1 mutant, L1(T202C), and a single-Cys L9 mutant, L9(Q18C), were designed, overexpressed, purified and labeled with Cy5- and Cy3-maleimide, respectively, as previously described^{4,6}. The Cy5-labeled L1 and Cy3-labeled L9 proteins were then reconstituted into the 50S subunits lacking L1 and L9, and the subunits were purified *via* sucrose density gradient ultracentrifugation^{4,6}.

mRNA preparation

All mRNAs used in the present study were derived from a previously described variant of an mRNA encoding the first 20 amino acids of gene product 32 from T4 bacteriophage⁷. Five mRNAs were designed such that their first codons code for fMet, Phe, Tyr, Glu, or Val, and no other codons that bind the anticodons of tRNA^{fMet}, tRNA^{Phe}, tRNA^{Tyr}, tRNA^{Glu}, or tRNA^{Val} are present in any reading frame (Supplementary Fig. 1). All mRNAs were *in vitro* transcribed from linearized plasmid DNA templates using T7 RNA polymerase following a previously described protocol^{6,8-10}. A 3'-biotinylated DNA oligonucleotide (TGTGTAAGTTTTAGGTTGATTTG-Biotin; Integrated DNA Technologies) complementary to the 5' end of the mRNAs was then hybridized to these mRNAs to enable surface immobilization as previously described^{6,10}. mRNA transcripts hybridized to a 3'-biotinylated DNA oligonucleotide are hereafter referred to as "biotin-mRNAs".

tRNA mutagenesis and purification

The pUC13.trnfM plasmid (a kind gift from Prof. Uttam RajBhandary, MIT) carrying the *E. coli metY* gene, which encodes tRNA^{fMet} isoacceptor 2, tRNA^{fMet₂(11)}, was mutated using the QuikChange Site-Directed Mutagenesis Kit (Stratagene) according to the manufacturer's instructions to generate tRNA^{fMet} isoacceptor 1, tRNA^{fMet₁}, and all tRNA^{fMet₂} mutants. tRNA^{fMet₂} mutants included: tRNA^{Anti} (G31A C39U), in which the G31-C39 base pair in the anticodon stem of tRNA^{fMet₂} is changed to the A31-U39 base pair found in tRNA^{Phe}; tRNA^{Acc} (C1G A72C), in which the mismatched C1•A72 base pair in the aminoacyl acceptor stem of tRNA^{fMet₂} is changed

to the G1-C72 Watson-Crick base pair found in tRNA^{Phe}; tRNA^{D-flip} (A11C U24G), in which the purine-pyrimidine A11-U24 base pair within the D stem of tRNA^{fMet₂} is flipped to the pyrimidine-purine C11-G24 base pair found in tRNA^{Phe}; tRNA^{D-dis} (A11C), in which the A11-U24 base pair within the D stem is disrupted by changing A11 to C11; and tRNA^{Acc/D-flip} (C1G A11C U24G A72C), in which the mutations generated in tRNA^{Acc} and tRNA^{D-flip} are combined.

All tRNAs were expressed in *E. coli* strain B105, which lacks the *metY* gene and therefore endogenous tRNA^{fMet₂}, and were purified using a previously published protocol¹²⁻¹⁴ with slight modifications. Briefly, tRNA^{fMet₁} and tRNA^{fMet₂} were separated from each other as well as from elongator tRNAs and all other cellular RNA species by native polyacrylamide gel electrophoresis (PAGE) on a 15 % (w/v) polyacrylamide gel prepared with TBE Buffer (89 mM Tris base, 89 mM boric acid and 2 mM ethylenediamine tetraacetic acid) and run in TBE Buffer at a constant voltage of 400 V for 24 hours at room temperature (Supplementary Fig. 2). tRNA bands were identified by UV shadowing at 254 nm wavelength, cut from the gel, and eluted from the gel slices using RNA Elution Buffer (10 mM Tris hydrochloride (pH_{25 °C} = 7.5), 1 mM ethylenediamine tetraacetic acid and 10 mM sodium chloride). A Phenyl 5PW TSK-Gel hydrophobic interaction chromatography (HIC) column (Tosoh Bioscience) was used to further purify the eluted tRNAs in the following manner. The eluted tRNAs were ethanol precipitated and resuspended in HIC Buffer A (1.7 M ammonium sulfate and 10 mM ammonium acetate, pH=6.3). These resuspended native PAGE-purified tRNAs were loaded onto a pre-equilibrated HIC column (equilibrated against 100% HIC Buffer A), and eluted from the HIC column using a 0-100 % gradient in HIC Buffer B (10 % (v/v) methanol and 10 mM ammonium acetate, pH=6.3) applied over a gradient length of 25 column volumes (Supplementary Fig. 3). All tRNA^{fMet₂} mutants were purified using the same protocols.

The combined A11C U24G mutations significantly change the migration of tRNA^{D-flip} and tRNA^{Acc/D-flip} on the native gel such that these tRNA mutants migrate within the region where elongator tRNAs typically migrate rather than at the position where wild-type tRNA^{fMet₂} migrates (Supplementary Fig. 2). It was therefore necessary to control for possible contamination of the tRNA^{D-flip} and tRNA^{Acc/D-flip} samples with elongator tRNAs, particularly tRNA^{Met} which could potentially bind to the AUG codon in our mRNA construct. To assess the level of possible contamination, the bands corresponding to the migration positions of tRNA^{D-flip} and tRNA^{Acc/D-flip} were cut out of a control lane of the native gel loaded with a crude RNA extract prepared from *E. coli* strain B105 which had not been transformed with the pUC13.trn^{fMet} plasmid. The tRNAs eluted from these bands (hereafter referred to as D-flip control tRNA and Acc/D-flip control tRNA) were subsequently ethanol precipitated and resuspended in HIC Buffer A. HIC analyses of the native PAGE-purified tRNA^{D-flip}, tRNA^{Acc/D-flip}, D-flip control tRNA, and Acc/D-flip control tRNA were then used to estimate that any potential contamination of tRNA^{D-flip} and tRNA^{Acc/D-flip} with elongator tRNAs was <2 % (Supplementary Fig. 3).

Aminoacylation and formylation analysis of wild-type tRNA^{fMet₁}, tRNA^{D-flip}, and D-flip control tRNA

Wild-type tRNA^{fMet₁} (Sigma-Aldrich), tRNA^{D-flip}, and D-flip control tRNA purified through the native PAGE and HIC procedures described above were subsequently analyzed for their aminoacylation and formylation activities. This analysis was used to determine if tRNA^{Met}, which

would compete with tRNA^{D-flip} for binding at the AUG codon of the mRNA construct during PRE^{A_{D-flip}} complex preparation, was present within the <2 % elongator tRNA contamination of the tRNA^{D-flip} sample.

300 pmol of each tRNA was 3'-labeled with α -³²P-ATP (Perkin Elmer) by reacting with 900 μ g of nucleotidyl transferase at 37 °C for 5 min in a total reaction volume of 30 μ L of ³²P labeling buffer (10 mM magnesium chloride, 50 μ M sodium diphosphate, and 50 mM glycine (pH = 9.0)). 3'-³²P-labeled tRNAs were then purified by phenol extraction, chloroform extraction and ethanol precipitation, and resuspended in water.

tRNA^{fMet}₁ was aminoacylated using methionyl-tRNA synthetase (MetRS) and formylated using methionyl-tRNA transformylase (MTF) as previously described⁶. Briefly, the 10-formyl-tetrahydrofolate formyl group donor was prepared in two steps. In the first step, 5:10-methenyltetrahydrofolate was prepared from folinic acid by dissolving 25 mg of the calcium salt of folinic acid (Acros Organics) in 2 mL of 50 mM 2-mercaptoethanol and then adding 220 μ L of 1 M hydrochloric acid to the reaction and incubating at room temperature for 3 hours until 5:10-methenyltetrahydrofolate crystallized. In the second step, 61 nmol of 5:10-methenyltetrahydrofolate was incubated in a buffer consisting of 87 mM potassium hydroxide and 43 mM Tris hydrochloride (pH_{25°C} = 7.5) in a total reaction volume of 5 μ L for 15 minutes at room temperature. For aminoacylation reactions only, 200 pmol of 3'-³²P-labeled tRNA^{fMet} was incubated with 800 pmol of methionine, and 0.2 pmol of MetRS in a total reaction volume of 10 μ L in AF Buffer (50 mM Tris hydrochloride (pH_{37°C} = 7.5), 7 mM magnesium chloride, 150 mM potassium chloride, 0.1 mM ethylenediamine tetraacetic acid, 1 mM dithiothreitol, and 2.5 mM ATP) for 10 min at 37 °C. Combined aminoacylation-formylation reactions were prepared identically to aminoacylation reactions with the exception that 3 nmol of 10-formyl-tetrahydrofolate and 2 pmol of MTF were included in the reaction mixture. The formylated and/or aminoacylated tRNAs were stabilized through the addition of 0.1 \times the reaction volume of 3 M sodium acetate (pH = 5.0) and purified by phenol extracting twice, chloroform extracting once, ethanol precipitating for 1 hour at -80 °C, centrifuging in a microfuge for 15 min at 14,000 \times g at 4 °C, and resuspending the resulting pellets in 10 mM potassium acetate (pH = 5.0).

Deacylated control tRNAs, aminoacylated tRNAs, and aminoacylated-formylated tRNAs were digested with P1 nuclease by combining 2 Units of P1 nuclease (Sigma-Aldrich) with 20 pmol of tRNA in a total reaction volume of 2.5 μ L of 200 mM sodium acetate (pH = 5.0) and incubating for 10 min at room temperature^{15,16}. P1 nuclease reactions were quenched with 9 \times the reaction volume of thin layer chromatography (TLC) buffer (5 % (v/v) acetic acid and 10 mM ammonium chloride). ~1 pmol of each tRNA was then spotted onto a 20 cm x 20 cm PEI-cellulose F TLC plate (EMD Chemicals Inc.) and run in TLC buffer for approximately 1 hour. The TLC plate was air dried, exposed to a phosphorimaging screen (Amersham Biosciences) overnight, and scanned using a Storm 860 phosphorimager (Molecular Dynamics). TLC spot intensities were quantified using ImageQuant software (Molecular Dynamics) (Supplementary Fig. 4). The results of this assay revealed that the <2 % elongator tRNA contamination of the tRNA^{D-flip} sample did not contain any detectable amount of tRNA^{fMet}.

Primer extension inhibition assay for verifying codon-specific binding of tRNAs into the P site

Analysis of the binding specificity of wild-type tRNAs and tRNA^{fMet}₂ mutants was

conducted using a slightly modified version of a previously described primer extension inhibition assay¹⁷⁻¹⁹. Briefly, a DNA primer (5'-AATTGCCGTTGAGCGATT-3', Integrated DNA Technologies) complementary to the 3' end of the mRNAs described above was radiolabeled on its 5' end using γ -³²P-ATP (Perkin Elmer) and T4 polynucleotide kinase (New England Biolabs) according to the manufacturer's instructions. The primer was then annealed to each mRNA by mixing 5 pmol of 5'-³²P-primer, 20 pmol of cold primer, and 50 pmol of the mRNA in a total reaction volume of 20 μ L of 25 mM Tris acetate (pH_{25 °C} = 7.5) and incubating for 2 minutes at 90 °C followed by slow cooling to room temperature. Primer-annealed mRNAs were assembled into PRE^A complexes with the appropriate wild-type tRNA or tRNA^{fMet}₂ mutant by first incubating 1.5 pmol of primer-annealed mRNA, 6 pmol of deacylated tRNA, and 3 pmol of 30S subunits in a total reaction volume of 4 μ L in Ribosome Assembly Buffer (50 mM Tris hydrochloride (pH_{25 °C} = 7.5), 70 mM ammonium chloride, 30 mM potassium chloride, 6 mM 2-mercaptoethanol, and 7 mM magnesium chloride) for 10 minutes at 37°C; this was followed by the addition of 3 pmol of 50S subunits and a second incubation for 20 min at 37°C. Primer-annealed mRNAs on the assembled PRE^A complexes were then reverse transcribed by adding 15 Units of AMV reverse transcriptase (Promega), 31.3 nmol ATP, and 15.6 nmol each of dGTP, dATP, dCTP, and dTTP, to the entire PRE^A complex assembly reaction prepared in the previous step in a total reaction volume of 25 μ L in Tris-polymix buffer at 10 mM magnesium acetate and incubating the reverse transcription reaction for 15 min at 37°C. Reverse transcription reactions were phenol extracted twice, chloroform extracted once, and ethanol precipitated. The resulting pellets were resuspended in Gel Loading Buffer (23 M formamide, 0.09% (w/v) bromophenol blue and 0.09% (w/v) xylene cyanol) and 5'-³²P-labeled cDNAs were analyzed on a 9 % (w/v) denaturing PAGE followed by phosphorimaging (Supplementary Fig. 5). The results of this assay demonstrated that all wild-type tRNAs and their associated mRNAs (Supplementary Fig. 1) efficiently formed PRE^A complexes in which the tRNA and its corresponding codon were properly positioned within the P site. The results also show that all tRNA^{fMet}₂ mutants and their associated AUG-containing mRNA (Supplementary Fig. 1) formed PRE^A complexes with efficiencies that were equivalent to that observed for wild-type tRNA^{fMet}₂ and that the tRNAs and the AUG codon were properly positioned into the P site.

Assembly and purification of PRE^A complexes

PRE^A complexes for smFRET experiments were assembled essentially as described above for the primer extension inhibition assays with the exception that the primer-annealed mRNA was replaced with biotin-mRNA. Briefly, a mixture of 30 pmol of biotin-mRNA, 20 pmol of deacylated tRNA, and 15 pmol of 30S subunits, in a total reaction volume of 30 μ L of Ribosome Assembly Buffer, was incubated for 10 min at 37 °C. 10 pmol of L1-L9-labeled 50S subunits were then added to the reaction followed by an additional incubation for 20 min at 37 °C. The reaction was then diluted to 100 μ L with Tris-polymix buffer at 26 mM magnesium acetate in order to bring the final concentration of magnesium ions in diluted reaction to 20 mM. PRE^A complexes prepared in this way were then layered on the top of a 10-40% (w/v) sucrose gradient prepared in Tris-polymix buffer at 20 mM magnesium acetate and purified by sucrose density gradient ultracentrifugation as previously described^{1,2}.

smFRET imaging using total internal reflection fluorescence microscopy

PRE^A complexes were tethered *via* their biotin-mRNA to the surface of a quartz microfluidic flowcell that had been passivated with a mixture of polyethyleneglycol (PEG) and PEG-biotin and derivatized with streptavidin^{1,2}. As previously described^{1,2}, smFRET imaging was performed with a laboratory-built, wide-field, prism-based total internal reflection fluorescence (TIRF) microscope using a 532 nm diode-pumped solid-state laser (CrystaLaser, Inc.) as an excitation source operating at an excitation power density of 22 W cm⁻² (the excitation area is estimated to be 0.05 mm²) and a 512 pixel × 512 pixel electron-multiplying charge-coupled-device camera (Cascade II 512:B, Photometrics, Inc.) as a detector operating with 2 × 2 pixel binning and a time resolution of 10 frames s⁻¹, unless otherwise indicated. The result is a 100 ms frame⁻¹ movie in which 200-300 single, spatially resolved PRE^A complexes are imaged within a 60 μm × 120 μm field of view. Movies were recorded over a time frame of ~50 seconds to ensure that the majority of fluorophores in the field of view were photobleached within the observation period. The dataset for each PRE^A complex typically consisted of 2-5 movies recorded from different fields of view within the same microfluidic flowcell. Three independent datasets were recorded for each PRE^A complex and all parameters (FRET efficiencies, equilibrium constants, transition rates, etc.) for each PRE^A complex were reported as the mean and the standard deviation based on the three independent datasets recorded.

Identification of single Cy3-Cy5 pairs and generation and idealization of single smFRET *versus* time trajectories

Individual Cy3-Cy5 pairs were identified and corresponding smFRET *versus* time trajectories were obtained and idealized as previously described^{1,20}. Briefly, single Cy5 fluorophores in each movie were first identified from the background noise by applying an intensity threshold to a single compiled image containing the maximum pixel value for each pixel across all but the first 20 frames of the movie. Exclusion of the first 20 frames of the movie from the compiled image ensured that only Cy5 fluorophores with lifetimes >2 s were identified by the threshold analysis. Alignment of the Cy3 and Cy5 halves of the compiled image then allowed identification and selection of the Cy3 fluorophore corresponding to each selected Cy5 fluorophore, thus providing the set of Cy3-Cy5 pairs for each movie. Using the identified Cy3-Cy5 pairs, Cy3-Cy5 emission intensity *versus* time trajectories were plotted and the selection of single Cy3-Cy5 pairs was verified by ensuring single-step photobleaching of the Cy3-Cy5 intensity trajectories. Individual Cy3-Cy5 intensity trajectories were baseline corrected and corrected for a small amount (~7%) of Cy3 signal bleedthrough into the Cy5 field of view, which is characteristic of the 680±25 nm Cy5 emission filter used in our TIRF microscope. Individual smFRET *versus* time trajectories were plotted from each baseline- and bleedthrough-corrected Cy3-Cy5 intensity trajectory by calculating the FRET efficiency at each time point using $E_{\text{FRET}} = I_{\text{Cy5}} / (I_{\text{Cy3}} + I_{\text{Cy5}})$, where E_{FRET} is the FRET efficiency and I_{Cy3} and I_{Cy5} are the Cy3 and Cy5 emission intensities, respectively. Raw smFRET *versus* time trajectories were then idealized using the vbFRET software program, which employs a maximum evidence-based model-selection algorithm for accurately determining the number of FRET states present in the data²⁰. The maximum number of FRET states that vbFRET attempted to fit was set to 5, and the number of fitting attempts to be made per smFRET trajectory was set to 25. As previously reported⁴, vbFRET finds that a two-state model provides the maximum evidence and is therefore the model that is best supported by the data. Comparison of the observed FRET efficiencies for the two states identified by vbFRET with the expected Cy3 to Cy5 distances

predicted from structural models of the open and closed conformations of the L1 stalk (kindly provided by H. Gao, X. Aguirrezabala, and J. Frank)^{21,22} allowed assignment of the two FRET states to the open and closed conformations of the L1 stalk⁴.

Calculation of GS1 \rightleftharpoons GS2 equilibrium constants and transition rates

For each dataset, the first 20 time points of each idealized smFRET *versus* time trajectory were extracted and plotted in a one-dimensional FRET histogram. The use of only the first 20 time points ensured that the histograms did not contain any 0 FRET efficiencies arising from observation periods in which Cy5 had photobleached but Cy3 continued to emit. The two observed peaks in the one-dimensional FRET histogram were fit to two Gaussian distributions using Origin 7.0 (OriginLab Corporation), with initial guesses for the centers of the Gaussian distributions set at 0.35 FRET (for the closed L1 stalk conformation, GS1) and 0.55 FRET (for the open L1 stalk conformation, GS2). High and low threshold values defining the window of FRET efficiencies that corresponded to the GS1 and GS2 states were set using the center and full width at half height (FWHM) of each Gaussian distribution.

The populations of GS1 (P_{GS1}) and GS2 (P_{GS2}) for each data set were determined by counting the number of time points that fell within the FRET efficiency window corresponding to each state. Only the first 20 time points of each smFRET trajectory were used to determine P_{GS1} and P_{GS2} in order to avoid bias in the populations arising from the unequal rates of fluorophore photobleaching from the GS1 and GS2 states⁴. The fractional populations of GS1 (% GS1) and GS2 (% GS2) reported in Table 1 were the relative percentages of P_{GS1} and P_{GS2} , respectively. The equilibrium constant, K_{eq} , reported in Table 1 was then calculated as $K_{eq} = P_{GS2}/P_{GS1}$.

Since transitions between FRET states separated by FRET efficiencies of less than 0.05 cannot generally be distinguished from noise, transitions identified by vbFRET that were composed of a change in FRET efficiency of less than 0.05 (< 1% of the total transitions identified by vbFRET) were disregarded. Using the FRET efficiency windows corresponding to GS1 and GS2, the dwell times spent in GS1 before transitioning to GS2 and the dwell times spent in GS2 prior to transitioning to GS1 were extracted from the individual idealized smFRET trajectories in each dataset and plotted as one-dimensional dwell-time histograms. The lifetimes of the GS1 and GS2 states were then determined by fitting the dwell-time histograms with single-exponential decays^{1,4}. $k_{GS1 \rightarrow GS2}$ and $k_{GS2 \rightarrow GS1}$ were calculated by taking the inverse of the GS1 and GS2 lifetimes, respectively, and correcting the resulting rates for the rates of fluorophore photobleaching from the GS1 and GS2 states, respectively, as previously described^{4,10,23}.

Calculation of slow transition rates using equilibrium constants

PRE^{-A}_{fMet-2} , PRE^{-A}_{Anti} and PRE^{-A}_{Acc} complexes exhibit extended lifetimes in GS1. In these complexes, the rate of photobleaching from GS1 effectively out-competes the slower rate of GS1 \rightarrow GS2 transitions (i.e. $k_{GS1 \rightarrow GS2}$) resulting in an increased number of smFRET trajectories in SP_{GS1} (Fig. 2 and Supplementary Table 1). To calculate the slow $k_{GS1 \rightarrow GS2}$ in these complexes in a manner more accurate than our standard dwell-time analysis, a slightly modified dwell-time analysis method was used. For these complexes, the GS2 lifetime and $k_{GS2 \rightarrow GS1}$ were determined using the standard dwell-time analysis described above. Assuming a two-state

model, $k_{GS1 \rightarrow GS2}$ could then be calculated from K_{eq} for the $GS1 \rightleftharpoons GS2$ equilibrium (determined as described in the previous section) using $k_{GS1 \rightarrow GS2} = k_{GS2 \rightarrow GS1} \times K_{eq}$.

Verification of transition rates for the slowest transitioning complex using smFRET *versus* time trajectories recorded at a decreased time resolution

To verify the accuracy with which the transition rates for the slowest-fluctuating PRE^A complex could be recovered by the dwell-time analysis described above, we recorded movies of the PRE^A complex exhibiting the slowest transitions, PRE^A_{Acc} , in which the laser excitation source was shuttered to provide a 150 ms exposure for each frame and a 450 ms time interval between frames, thus yielding a time resolution of 600 ms frame⁻¹. This amounted to an approximately 6-fold reduction in the time resolution of the experiment (10 frames s⁻¹ for continuous excitation experiments *versus* 1.7 frames s⁻¹ in the shuttering experiments) as well as an approximately 4-fold reduction in the rates of Cy3 and Cy5 photobleaching and, consequently, an approximately 4-fold increase in the total observation time. Single Cy3-Cy5 pairs were identified and smFRET trajectories were obtained and idealized using the procedures outlined above. Both $k_{GS1 \rightarrow GS2}$ and $k_{GS2 \rightarrow GS1}$ were determined directly from dwell-time analyses with further corrections for the rate of fluorophore photobleaching from the GS1 and GS2 states calculated from the shuttered movies. Values of $k_{GS1 \rightarrow GS2}$ and $k_{GS2 \rightarrow GS1}$ obtained in this way were 0.06 s⁻¹ and 0.16 s⁻¹, respectively, in almost perfect agreement with the corresponding values for $k_{GS1 \rightarrow GS2}$ and $k_{GS2 \rightarrow GS1}$ calculated from dwell-time analyses and the equilibrium constant using movies recorded under continuous laser excitation (0.06 s⁻¹ and 0.15 s⁻¹, respectively) (Table 1). Based on this control experiment, we conclude that dwell-time analysis with photobleaching correction and calculation of rate constants from K_{eq} are robust methods for measuring the true transition rates even for slow-transitioning PRE^A complexes.

SUPPLEMENTARY DISCUSSION

The conformation of the L1 stalk, intersubunit orientation of the ribosome, and configuration of the P-site tRNA are coupled within the GS1 \rightleftharpoons GS2 equilibrium

As we state in the main text, the population distribution between the open and closed L1 stalk conformations for individual PRE^{-A} complexes depends on the identity of the P-site bound tRNA (Fig. 3). Previously, Cornish *et al* used an smFRET signal reporting on intersubunit rotation²⁴, to examine the population distribution between non-rotated and rotated intersubunit orientations for a subset of PRE^{-A} complexes that partially overlaps with the subset in this study (PRE^{-A}_{fMet-1}, PRE^{-A}_{Phe}, and PRE^{-A}_{Tyr}). Comparison of our results with those from Cornish *et al* demonstrates that the tRNA-dependent trend we find in the equilibrium constants (K_{eqS}) describing the equilibrium between the open and closed L1 stalk conformations (Table 1) in these PRE^{-A} complexes mirrors that observed in the K_{eqS} describing the equilibrium between the non-rotated and rotated intersubunit orientations in the analogous PRE^{-A} complexes. Unfortunately, differences in experimental conditions, strains of *E. coli* used as a source of ribosomal subunits, and origins of the 30S subunit (*in vivo* assembled *versus in vitro* reconstituted)—all factors which have been shown to affect the thermodynamic and kinetic parameters governing tRNA and ribosome dynamics within PRE^{-A} complexes²⁴⁻²⁶—preclude a detailed comparison of the absolute values of these parameters between the two studies. Nevertheless, this observation demonstrates that the identity of the P-site tRNA influences the propensity of the L1 stalk to adopt the open or closed conformation in a manner that correlates with the propensity of the ribosome to adopt the non-rotated or rotated intersubunit orientation, respectively.

Along similar lines, Dorner *et al* have previously shown that, relative to wild-type tRNA^{fMet}, a C1G A72C mutant tRNA^{fMet} analogous to the acceptor stem mutant tRNA^{Acc} which we have investigated here (described in the sub-section entitled “5'-terminal base pairing in acceptor stem decreases $k_{\text{GS2} \rightarrow \text{GS1}}$ ” in the Results section of the main text) preferentially occupies the P/E configuration within PRE complexes²⁷. Mirroring this result, we find that, relative to PRE^{-A}_{fMet-2} complexes, PRE^{-A}_{Acc} complexes exhibit a higher occupancy of the closed L1 stalk conformation. Once again, comparison of these results demonstrates that the identity of the P-site tRNA influences the propensity of the L1 stalk to adopt the open or closed conformation in a manner that correlates with the propensity of the P-site tRNA to adopt the P/P or P/E configuration, respectively. Collectively, these comparisons support the view that the conformation of the L1 stalk, the subunit orientation of the ribosome, and the configuration of the tRNAs within PRE complexes are coupled within the context of the GS1 \rightleftharpoons GS2 equilibrium^{1,28}.

Sequence alterations within the D stem and/or variable loops of tRNA^{fMet} lead to alterations in the stability of P/P tRNA^{fMet} that ultimately modulate $k_{\text{GS1} \rightarrow \text{GS2}}$

As described in the main text, our data demonstrate that PRE^{-A}_{fMet-2}, PRE^{-A}_{D-flip}, PRE^{-A}_{D-dis}, and PRE^{-A}_{fMet-1} exhibit values of $k_{\text{GS1} \rightarrow \text{GS2}}$ that are sensitive to the minor sequence differences located within the D stems and/or variable loops of tRNA^{fMet}₂, tRNA^{D-flip}, tRNA^{D-dis}, and tRNA^{fMet}₁. Interpreting our results within the context provided by comparative structural analyses^{29,30} and previous biochemical studies³¹ (see main text) strongly suggests that, rather than differentially modulating specific tRNA-ribosome interactions, the sequence differences among these tRNAs

translate into slight differences in the stabilities of these tRNAs when they are bound within the P/P configuration and that these differences in stability underlie the observed differences in the values of $k_{GS1 \rightarrow GS2}$ of these PRE^{-A} complexes. The notion that the relatively subtle differences in the sequences within the D stems and variable loops of $tRNA^{fMet}_2$, $tRNA^{D-flip}$, $tRNA^{D-dis}$, and $tRNA^{fMet}_1$ can lead to differences in the structural stabilities of these tRNAs is strengthened by their distinct migrations on a native gel. Although it is difficult to quantitatively correlate the migration patterns of the tRNAs on a native gel with their structural stabilities, the very fact that we observe differences in the migration patterns of $tRNA^{fMet}_2$, $tRNA^{D-flip}$, $tRNA^{D-dis}$, and $tRNA^{fMet}_1$ indirectly supports our proposal that sequence alterations within the D stems and variable loops alter the stabilities of these tRNAs. Notably, the difference between the migration of $tRNA^{D-flip}$, whose corresponding PRE^{-A}_{D-flip} complex exhibits the fastest $k_{GS1 \rightarrow GS2}$, and the other three tRNAs is particularly striking.

The intrinsic conformational flexibility of the P-site tRNA may influence its transition from the P/P to the P/E configuration

As described in the main text, the effects that altering individual tRNA structural features have on PRE^{-A} complex dynamics can be interpreted in terms of the ability of each alteration to stabilize or destabilize GS1 and/or GS2. Interpreted within this framework, we have concluded that the intrinsic conformational flexibility of the P/P tRNA modulates the stability of GS1 (see the discussion in the main text and above). In addition to its role in modulating the stability of GS1, it is also possible that the intrinsic conformational flexibility of the P-site tRNA may directly influence its transition from the P/P to the P/E configuration. Structural studies have revealed that tRNAs exhibit a pronounced distortion at the junction between the D and anticodon stems when bound to the ribosome in the P/P configuration^{29,30,32-34}. More specifically, the D stem of the P/P tRNA is partially unwound relative to its anticodon stem and the tRNA is kinked at a hinge formed by the G26-A44 base pair at the junction between the anticodon and D stems such that it is positioned towards the 50S subunit and slightly towards the A site^{29,30,34} (Fig. 6b). Molecular dynamics simulations³⁵ suggest that this junction has to be remodeled as the P-site tRNA moves from its P/P to its P/E configuration, likely leading to a “relaxation” of the tRNA structure such that it more closely resembles the conformation that is observed in ribosome-free tRNA (Fig. 6b). Remodeling of this distortion may therefore be an important determinant of the rate of the GS1→GS2 transition and, consequently, translocation.

tRNA-mediated control of PRE complex dynamics may play a role in translational regulation

Despite their differences relative to PRE^{-A}_{fMet} complexes and their similarities relative to PRE^{-A}_{Phe} complexes, it is important to note that each PRE^{-A}_{elong} complex we have investigated does exhibit unique GS1↔GS2 dynamics (Table 1). Based on the discussion in the main text and above, we expect that subtle differences in the structure of each elongator tRNA species will differentially alter the GS1↔GS2 equilibrium of PRE complexes carrying particular elongator tRNAs at the P site and, consequently, will differentially regulate the translocation kinetics of these PRE complexes. It follows that the use of particular tRNAs at particular codons within an mRNA may serve as an additional regulatory mechanism, allowing the rate of translation

elongation to be tuned with single codon resolution. For example, the PRE^A complex carrying tRNA^{Tyr}, which has a disrupted base pair within the D stem and an extended variable loop, exhibits the fastest $k_{GS1 \rightarrow GS2}$ and slowest $k_{GS2 \rightarrow GS1}$ in our study, thus yielding the GS1 \rightleftharpoons GS2 equilibrium that was most shifted towards GS2; this suggests that PRE complexes carrying P-site tRNA^{Tyr} should be particularly efficient substrates for EF-G-promoted translocation.

Moreover, the P-site tRNA plays a critical role in maintaining the translational reading frame³⁶. In addition to alterations in the basepairing interactions between tRNA anticodons and mRNA codons at the P site, alterations in the aminoacyl acceptor stems, D stems, and variable loops of numerous tRNA species have been shown to trigger ribosomal frameshifting³⁶. It is therefore possible that tRNA-mediated control of the GS1 \rightleftharpoons GS2 equilibrium may somehow contribute to the fidelity of translocation and to the regulation of programmed ribosomal frameshifting events that modulate the expression of numerous genes^{37,38}. In summary, tRNA-mediated control of the GS1 \rightleftharpoons GS2 equilibrium may provide an additional level of translational regulation by enabling codon-dependent attenuation of the rate and accuracy of EF-G-promoted translocation. Further single-molecule studies of the kinetics and fidelity of translation elongation with single codon resolution, such as those recently reported by Wen *et al.*³⁹ and Uemura *et al.*⁴⁰, should allow testing of this hypothesis.

References

1. Fei, J., Kosuri, P., MacDougall, D.D. & Gonzalez, R.L., Jr. Coupling of ribosomal L1 stalk and tRNA dynamics during translation elongation. *Mol Cell* **30**, 348-59 (2008).
2. Blanchard, S.C., Kim, H.D., Gonzalez, R.L., Jr., Puglisi, J.D. & Chu, S. tRNA dynamics on the ribosome during translation. *Proc Natl Acad Sci U S A* **101**, 12893-8 (2004).
3. Stone, M.D. et al. Stepwise protein-mediated RNA folding directs assembly of telomerase ribonucleoprotein. *Nature* **446**, 458-61 (2007).
4. Fei, J. et al. Allosteric collaboration between elongation factor G and the ribosomal L1 stalk directs tRNA movements during translation. *Proc Natl Acad Sci U S A* **106**, 15702-7 (2009).
5. Gonzalez, R.L., Jr., Chu, S. & Puglisi, J.D. Thiostrepton inhibition of tRNA delivery to the ribosome. *RNA* **13**, 2091-7 (2007).
6. Fei, J. et al. A highly-purified, fluorescently-labeled *in vitro* translation system for single-molecule studies of protein synthesis. *Methods in Enzymology* **472**, 221-59 (2010).
7. Alberts, B.M. & Frey, L. T4 bacteriophage gene 32: a structural protein in the replication and recombination of DNA. *Nature* **227**, 1313-8 (1970).
8. Milligan, J.F., Groebe, D.R., Witherell, G.W. & Uhlenbeck, O.C. Oligoribonucleotide synthesis using T7 RNA polymerase and synthetic DNA templates. *Nucleic Acids Res* **15**, 8783-98 (1987).
9. Wyatt, J.R., Chastain, M. & Puglisi, J.D. Synthesis and purification of large amounts of RNA oligonucleotides. *Biotechniques* **11**, 764-9 (1991).
10. Sternberg, S.H., Fei, J., Prywes, N., McGrath, K.A. & Gonzalez, R.L., Jr. Translation factors direct intrinsic ribosome dynamics during translation termination and ribosome recycling. *Nat Struct Mol Biol* **16**, 861-8 (2009).
11. Ishii, S., Kuroki, K. & Imamoto, F. tRNAMetf2 gene in the leader region of the nuaA operon in Escherichia coli. *Proc Natl Acad Sci U S A* **81**, 409-13 (1984).
12. Lee, C.P., Mandal, N., Dyson, M.R. & RajBhandary, U.L. The discriminator base influences tRNA structure at the end of the acceptor stem and possibly its interaction with proteins. *Proc Natl Acad Sci U S A* **90**, 7149-52 (1993).

13. Mandal, N., Mangroo, D., Dalluge, J.J., McCloskey, J.A. & Rajbhandary, U.L. Role of the three consecutive G:C base pairs conserved in the anticodon stem of initiator tRNAs in initiation of protein synthesis in *Escherichia coli*. *RNA* **2**, 473-82 (1996).
14. Mandal, N. & Rajbhandary, U.L. *Escherichia coli* B lacks one of the two initiator tRNA species present in *E. coli* K-12. *J Bacteriol* **174**, 7827-30 (1992).
15. Ledoux, S. & Uhlenbeck, O.C. [3'-32P]-labeling tRNA with nucleotidyltransferase for assaying aminoacylation and peptide bond formation. *Methods* **44**, 74-80 (2008).
16. Wolfson, A.D. & Uhlenbeck, O.C. Modulation of tRNAAla identity by inorganic pyrophosphatase. *Proc Natl Acad Sci U S A* **99**, 5965-70 (2002).
17. Hartz, D., McPheeters, D.S., Traut, R. & Gold, L. Extension inhibition analysis of translation initiation complexes. *Methods Enzymol* **164**, 419-25 (1988).
18. Joseph, S. & Noller, H.F. EF-G-catalyzed translocation of anticodon stem-loop analogs of transfer RNA in the ribosome. *EMBO J* **17**, 3478-83 (1998).
19. Fredrick, K. & Noller, H.F. Accurate translocation of mRNA by the ribosome requires a peptidyl group or its analog on the tRNA moving into the 30S P site. *Mol Cell* **9**, 1125-31 (2002).
20. Bronson, J.E., Fei, J., Hofman, J.M., Gonzalez, R.L., Jr. & Wiggins, C.H. Learning rates and states from biophysical time series: a Bayesian approach to model selection and single-molecule FRET data. *Biophys J* **97**, 3196-205 (2009).
21. Valle, M. *et al.* Locking and unlocking of ribosomal motions. *Cell* **114**, 123-34 (2003).
22. Agirrezabala, X. *et al.* Visualization of the hybrid state of tRNA binding promoted by spontaneous ratcheting of the ribosome. *Mol Cell* **32**, 190-7 (2008).
23. Bartley, L.E., Zhuang, X., Das, R., Chu, S. & Herschlag, D. Exploration of the transition state for tertiary structure formation between an RNA helix and a large structured RNA. *J Mol Biol* **328**, 1011-26 (2003).
24. Cornish, P.V., Ermolenko, D.N., Noller, H.F. & Ha, T. Spontaneous intersubunit rotation in single ribosomes. *Mol Cell* **30**, 578-88 (2008).
25. Kim, H.D., Puglisi, J.D. & Chu, S. Fluctuations of transfer RNAs between classical and hybrid states. *Biophys J* **93**, 3575-82 (2007).
26. Munro, J.B., Altman, R.B., O'Connor, N. & Blanchard, S.C. Identification of two distinct hybrid state intermediates on the ribosome. *Mol Cell* **25**, 505-17 (2007).
27. Dorner, S., Brunelle, J.L., Sharma, D. & Green, R. The hybrid state of tRNA binding is an authentic translation elongation intermediate. *Nat Struct Mol Biol* **13**, 234-41 (2006).
28. Frank, J. & Gonzalez, R.L., Jr. Structure and dynamics of a processive brownian motor: the translating ribosome. *Annu Rev Biochem* **79**, 381-412 (2010).
29. Korostelev, A., Trakhanov, S., Laurberg, M. & Noller, H.F. Crystal structure of a 70S ribosome-tRNA complex reveals functional interactions and rearrangements. *Cell* **126**, 1065-77 (2006).
30. Selmer, M. *et al.* Structure of the 70S ribosome complexed with mRNA and tRNA. *Science* **313**, 1935-42 (2006).
31. Ali, I.K., Lancaster, L., Feinberg, J., Joseph, S. & Noller, H.F. Deletion of a conserved, central ribosomal intersubunit RNA bridge. *Mol Cell* **23**, 865-74 (2006).
32. Villa, E. *et al.* Ribosome-induced changes in elongation factor Tu conformation control GTP hydrolysis. *Proc Natl Acad Sci U S A* **106**, 1063-8 (2009).
33. Schmeing, T.M. *et al.* The crystal structure of the ribosome bound to EF-Tu and aminoacyl-tRNA. *Science* **326**, 688-94 (2009).
34. Korostelev, A. & Noller, H.F. The ribosome in focus: new structures bring new insights. *Trends Biochem Sci* **32**, 434-41 (2007).
35. Li, W. & Frank, J. Transfer RNA in the hybrid P/E state: correlating molecular dynamics simulations with cryo-EM data. *Proc Natl Acad Sci U S A* **104**, 16540-5 (2007).

36. Atkins, J.F. & Bjork, G.R. A gripping tale of ribosomal frameshifting: extragenic suppressors of frameshift mutations spotlight P-site realignment. *Microbiology and Molecular Biology Reviews* **73**, 178-210 (2009).
37. Atkins, J.F. *et al.* Overriding standard decoding: implications of recoding for ribosome function and enrichment of gene expression. *Cold Spring Harb Symp Quant Biol* **66**, 217-32 (2001).
38. Baranov, P.V., Gesteland, R.F. & Atkins, J.F. P-site tRNA is a crucial initiator of ribosomal frameshifting. *RNA* **10**, 221-30 (2004).
39. Wen, J.D. *et al.* Following translation by single ribosomes one codon at a time. *Nature* **452**, 598-603 (2008).
40. Uemura, S. *et al.* Real-time tRNA transit on single translating ribosomes at codon resolution. *Nature* **464**, 1012-7 (2010).